Metals and Materials International (2022) 28:523–533
https://doi.org/10.1007/s12540-021-01063-x

Improvement on Mechanical Properties of a bcc Matrix $Al_8(FeCuCrMn)_{92}$ High-Entropy Alloy by Phase Modulation of Interstitial Carbon Element

Conghui Hu[1] · Jianlei Zhang[1] · Yunhu Zhang[1] · Ke Han[2] · Changjiang Song[1] · Qijie Zhai[1]

Received: 7 April 2021 / Accepted: 7 June 2021 / Published online: 28 September 2021
© The Korean Institute of Metals and Materials 2021

Abstract
High-entropy alloys (HEAs) are novel multi-element alloys based on five or more constituent elements in a range of 5–35 at%. Here we present a method to improve strength of a body-centered cubic (bcc) matrix HEA without loss of ductility. The improvement was achieved by phase modulation combined other strengthening effect of interstitial carbon addition. Carbon addition can enhance strength and retain good ductility in some steels because carbon increases the volume fraction of face-centered cubic (fcc) phase. We used the same principle to design and fabricate a set of $Al_8(FeCuCrMn)_{92}C_x$ (x = 0, 1, 2, 3, 4 at%) HEAs under near-rapid solidification. Our results showed that carbon addition modulated constituent phases by increasing the volume fraction of fcc phase and carbides. As a result, addition of carbon increased yield strength of this bcc matrix HEA. But the ductility decreased, especially when carbon content was higher than 3 at%, which was ascribed to uneven distribution of Cu-rich fcc phase and carbides precipitated in bcc phase region. After annealing at 1173 K for 2 h, addition of 1 at% carbon improved yield strength without compressive fracture. It demonstrated that a proper carbon content addition with annealing can enhance the yield strength without loss of ductility for this bcc matrix HEA. Thus, interstitial carbon addition is a meaningful method to improve the mechanical properties by phase modulation combined other strengthening effect.

Keywords High-entropy alloys · Bcc matrix · Phase modulation · Interstitial carbon

1 Introduction

High-entropy alloys (HEAs) contain multi-principal elements in a range of 5–35 at%, which is an extraordinary alloying design paradigm [1–4]. HEAs show a great potential for application in many fields due to high fatigue resistance [5, 6], wear resistance [7], irradiation resistance [8], and other physical properties [9, 10]. The solid-solution phase is usually the main constituent phase in HEAs, which is different from traditional physical metallurgy theories [11]. In general, the most broadly investigated phases are body-centered cubic (bcc) and face-centered cubic (fcc) [12, 13].

It is difficult to further improve comprehensive mechanical properties in bcc-structured HEAs, because an increase of strength usually comes at the price of sacrificing ductility and vice versa [3, 4, 14–17]. For instance, Zhou et al. [15] enhanced the compressive strength of a bcc-structured AlCoCrFeNi HEA by introducing solid solution effect of Ti element but decreased its ductility from 26.9 to 5.3%. On the other hand, some improvement measures were only for ductility rather than strength. For example, based on the electron theory, Sheikh et al. [16] designed a bcc-structured HEA with an elongation of near 20%, while its fracture strength was lower than conventional refractory alloys. Huang et al. [17] improved ductility of $Ta_xHfZrTi$ from 4 to 27% by using transformation-induced ductility effect but led to a reduction of 400 MPa in strength. However, the ways to increase simultaneously both strength and ductility were seldom reported, except for grain refining [18].

Instead of adding substitutional elements, addition of interstitial elements is also an important method to tune

✉ Changjiang Song
riverssong@shu.edu.cn; riversxiao@163.com

[1] Center for Advanced Solidification Technology (CAST), School of Materials Science and Engineering, Shanghai University, Shanghai 200444, People's Republic of China

[2] National High Magnetic Field Laboratory, Florida State University, Tallahassee, FL 32310, USA

structures and properties of HEAs. Among them, carbon addition is widely studied [19, 20], e.g. Wang et al. [21] improved fracture strength of a fcc-structured FeNiMnAlCr HEA from 381 to 754 MPa by adding 1.1 at% interstitial carbon to obtain much higher lattice friction stress. Adding a certain content of carbon would promote formation of nano-sized carbides and improve strength of the equiatomic CoCrFeMnNi HEA by precipitation strengthening [22]. Furthermore, carbon can increase the fraction of austenite and improve ductility in some steels, which is really impressive [23]. Recently, it was confirmed that carbon addition also can increase fraction of fcc phase in some bcc matrix HEAs [24–26]. Thus, the achievement of a strength improvement in a bcc matrix HEA without loss of ductility by phase modulation of interstitial carbon element, is of great possibility. By addition of carbon, researchers had achieved compressive fracture strain of 48.8% in $(AlFeCoNi)_{98}C_2$ HEA [26], which contained several expensive alloying elements. Therefore, lower cost and higher ductility are desired in similar alloys.

We selected more common 3d transition metal elements (Fe, Cu, Cr and Mn) for our studies [27–29]. Using an inexpensive bcc matrix $Al_8(FeCuCrMn)_{92}$ HEA as a templet, we added interstitial carbon element to improve strength, while maintaining good ductility. The microstructures and mechanical properties of the $Al_8(FeCuCrMn)_{92}C_x$ (x = 0, 1, 2, 3, 4 at%) alloys were studied in this work.

2 Materials and methods

Alloy ingots with nominal compositions of $Al_8(FeCuCrMn)_{92}C_x$ (x = 0, 1, 2, 3, 4 at%) HEAs were made by cold-crucible levitation melting. The purity of Al, Fe, Cu, Cr, Mn and C (graphite) was above 99.9%. The composition homogenization was ensured by repeated melting at least four times. Strips in size of 60 mm × 60 mm × 2.5 mm were made by centrifugal casting under near-rapid solidification in an Ar atmosphere, which was described in detail in previous papers [25, 30]. Several samples were annealed at 1173 K for 2 h to eliminate thermal stress and obtain stable phases according to some reports [31–33]. Phase characterization was performed by X-ray diffraction (XRD), microstructures were characterized by using scanning electron microscopy (SEM) and electron probe microscopic analyzer (EPMA). Image analysis method have been used to quantitative assess phase fraction by Image J. The specimens for transmission electron microscopy (TEM) were prepared by using a twin-jet electrolytic polishing in a mixed solution of 10 vol% perchloric acid and 90 vol% alcohol. The cylindrical specimens with dimension of Φ 2 mm × 4 mm were prepared for compression tests at room temperature. At least three specimens for each strip were tested at a strain rate of 10^{-3} s^{-1}.

3 Results and Discussion

3.1 Phase Constitution and Microstructures

3.1.1 Microstructure of As-Cast Strips

Figure 1 shows XRD patterns of the as-cast $Al_8(FeCuCrMn)_{92}C_x$ (denoted as Cx hereafter) HEA strips. In the C0 strip, XRD showed both bcc and fcc phases, with the bcc phase as the matrix. In the C1 and C2 strips, the intensity of the diffraction peak for fcc phase were greater than that of the C0 strip, indicating that interstitial carbon element addition had promoted the formation of fcc phase. Thus, carbon addition modulated constituent phases of these alloys. A peak at around 44°, identified as $M_{23}C_6$ carbides, appears in the C3 strip, suggesting the formation of a small amount of carbides. When the carbon content was increased to 4 at%, the intensity of the diffraction peak for carbides is enhanced, indicating that the amount of carbides increased as carbon content increased.

Figure 2 presents SEM back-scatter images of the as-cast $Al_8(FeCuCrMn)_{92}C_x$ HEA strips. The C0 strip exhibited a flower-like structure, as shown in Fig. 2a1 and a2. SEM results showed distinct dark and bright regions. According to the XRD patterns, the dark region was bcc phase and the bright region was fcc phase. As carbon content increased, the fcc phase region expanded. Image analysis showed that the fraction of fcc phase increases from 17 vol% in the C0 strip to 33 vol% in the C4 strip. This quantitatively confirms that carbon addition had modulate constituent phases by the formation of fcc phase in the as-cast $Al_8(FeCuCrMn)_{92}C_x$ HEA strips. After carbon addition, however, some bcc phase

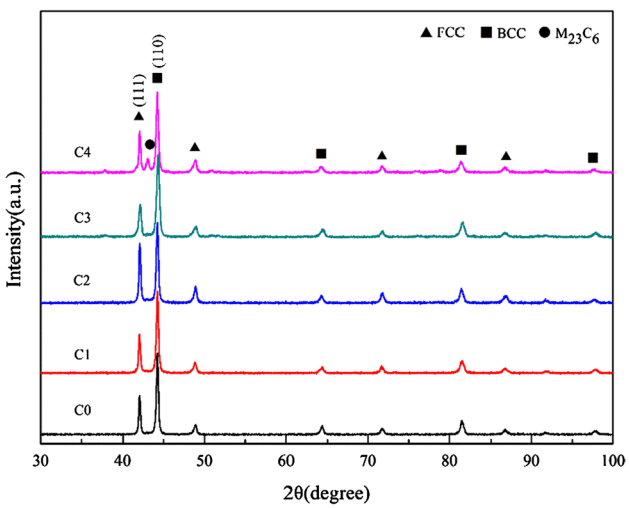

Fig. 1 XRD patterns of the as-cast $Al_8(FeCuCrMn)_{92}C_x$ (marked as Cx) HEA strips

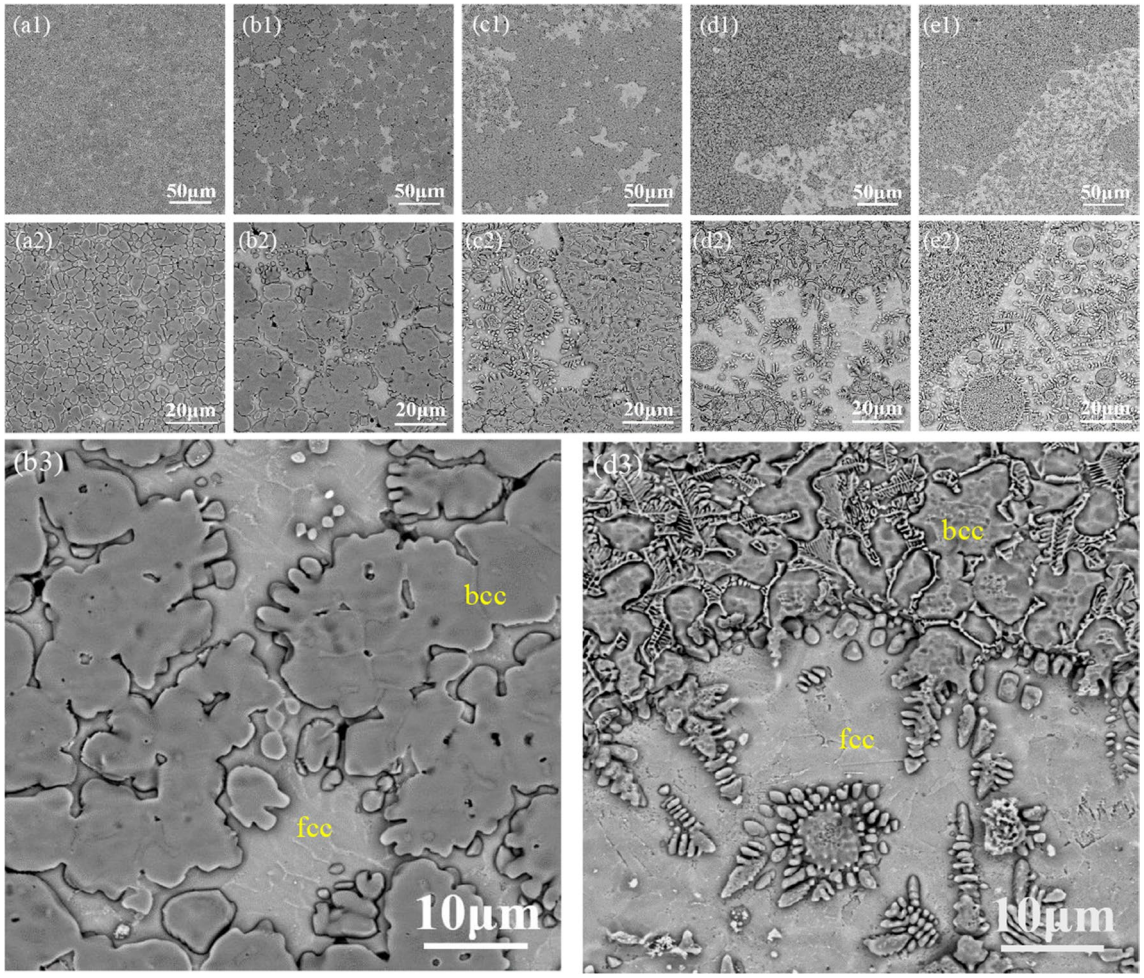

Fig. 2 Back scattering electron images of the as-cast $Al_8(FeCuCrMn)_{92}C_x$ (marked as Cx) HEA strips: **a1, a2** for C0 strip, **b1–b3** for C1 strip, **c1**, **c2** for C2 strip, **d1–d3** for C3 strip, **e1**, **e2** for C4 strip

grains began to aggregate and embed in the fcc phase region. With the addition of carbon, needle-like or fishbone-like precipitations arose in the bcc phase region. The distribution of fcc phase became more uneven when the carbon content was above 2 at%. The fraction of fcc phase increased as carbon content increased, but the uneven distribution of fcc phase became more pronounced when carbon content reached 3 at%.

To investigate the distribution of elements and precipitated phases in the as-cast $Al_8(FeCuCrMn)_{92}C_x$ HEA strips, we examined all of the samples using EPMA. Figure 3 displays elemental distribution maps of the C1 strip and the C3 strips. Chemical compositions of bcc and fcc phases in the as-cast strips are listed in Table 1. Elemental distribution maps of the C1 and C3 strips showed that the bcc phase was rich in Fe and Cr but poor in Cu, whereas the fcc phase was rich in Cu but poor in Fe and Cr in all strips. The bcc phase contained only 3 at% Cu, while the fcc phase contained over 60 at% Cu. In the C0 strip, the content of Al and Mn in the fcc phase was higher than that in the bcc phase, and the difference in Al and Mn content between fcc phase and bcc phases decreased after carbon addition. In the center of the bcc phase, Al and Mn were poor. Based on both morphology analysis and chemistry mapping, it is concluded that the precipitated phase appearing in the bcc phase region was rich in C and Cr, and should be considered a chromium carbide. It is also deduced that the carbides began to appear in the C1 strip, but its amount is too low to be detected by XRD.

To obtain the detailed information of carbides, TEM analysis was performed on the C1 strip. TEM image of the C1 strip is shown in Fig. 4. Both bright field (BF) and selected-area electron diffraction patterns (SADPs) showed that the C1 strip consisted of elongated fcc particles embedded in a bcc matrix. Figure 5a presents a BF TEM image of the chromium carbides. Figure 5b shows SADP taken along [111] zone axis and the dark field (DF) image from (022) is shown in Fig. 5c. It is indicated that

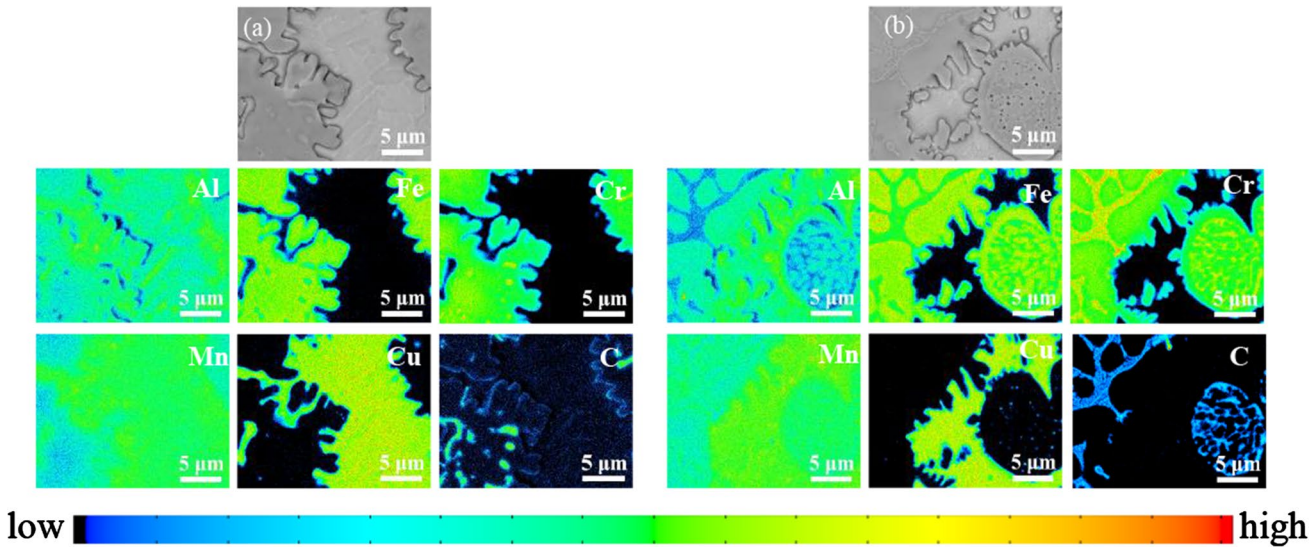

Fig. 3 Elemental distribution maps of the as-cast $Al_8(FeCuCrMn)_{92}C_1$ and $Al_8(FeCuCrMn)_{92}C_3$ HEA strips: **a** C0 strip, **b** C3 strip

Table 1 Chemical compositions of bcc and fcc phases in the as-cast $Al_8(FeCuCrMn)_{92}C_x$ HEAs derived from EPMA-EDS (since limited accuracy for light elements, carbon content is not listed here)

Sample	Phase	Al (at%)	Fe (at%)	Cu (at%)	Cr (at%)	Mn (at%)
C0	bcc	5.6 ± 0.7	33.9 ± 0.9	2.7 ± 0.2	39.3 ± 2.5	18.5 ± 1.5
	fcc	9.3 ± 1.7	3.1 ± 0.4	61.1 ± 0.9	2.4 ± 0.2	24.1 ± 1.2
C1	bcc	6.3 ± 1.4	34.0 ± 1.8	3.3 ± 0.4	36.0 ± 3.5	20.4 ± 2.7
	fcc	8.5 ± 1.3	2.9 ± 0.2	61.7 ± 1.7	1.9 ± 0.2	25.0 ± 0.7
C2	bcc	7.1 ± 1.6	34.9 ± 1.3	4.2 ± 0.5	31.3 ± 3.9	22.5 ± 1.7
	fcc	8.9 ± 1.1	2.3 ± 0.3	62.4 ± 1.3	1.5 ± 0.2	24.9 ± 1.0
C3	bcc	7.6 ± 1.0	36.4 ± 1.6	3.7 ± 0.8	29.8 ± 3.3	22.5 ± 1.4
	fcc	7.3 ± 0.5	2.8 ± 0.3	64.2 ± 1.7	1.9 ± 0.2	23.9 ± 1.2
C4	bcc	8.9 ± 1.6	37.0 ± 1.8	2.9 ± 0.8	27.3 ± 3.8	23.8 ± 2.1
	fcc	8.3 ± 0.8	2.4 ± 0.5	63.6 ± 0.7	1.6 ± 0.4	24.1 ± 1.0

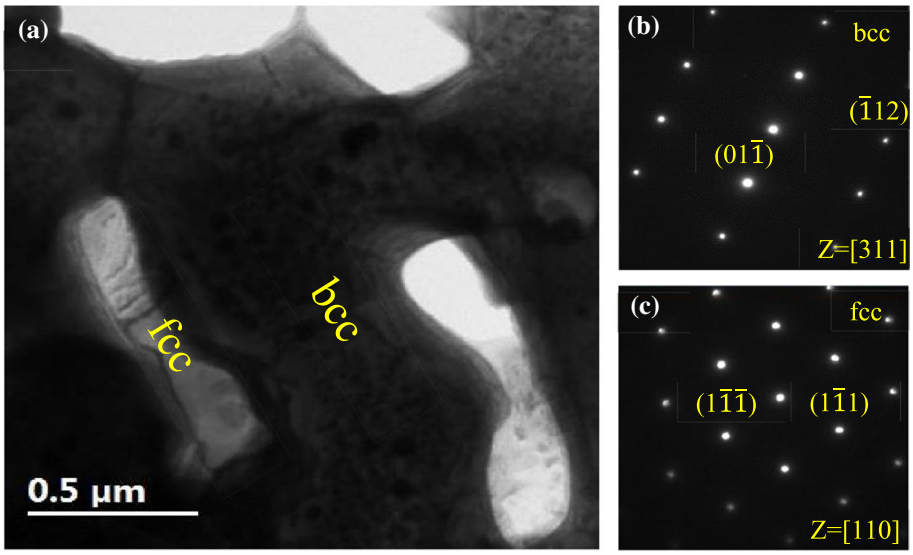

Fig. 4 TEM images of the as-cast $Al_8(FeCuCrMn)_{92}C_1$ HEA strip: **a** BF image of the matrix, **b** the SADP along [311] zone axis, **c** the SADP along [110] zone axis

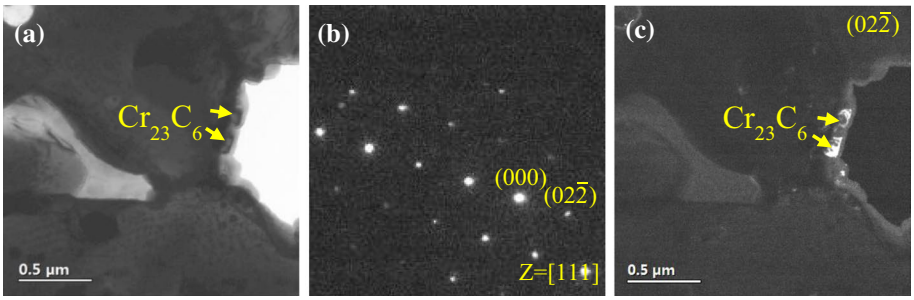

Fig. 5 TEM micrographs of submicron $Cr_{23}C_6$ in the as-cast $Al_8(FeCuCrMn)_{92}C_1$ HEA strip: **a** BF image of $Cr_{23}C_6$, **b** the SADP along [111] zone axis, **c** DF from (022) of $Cr_{23}C_6$

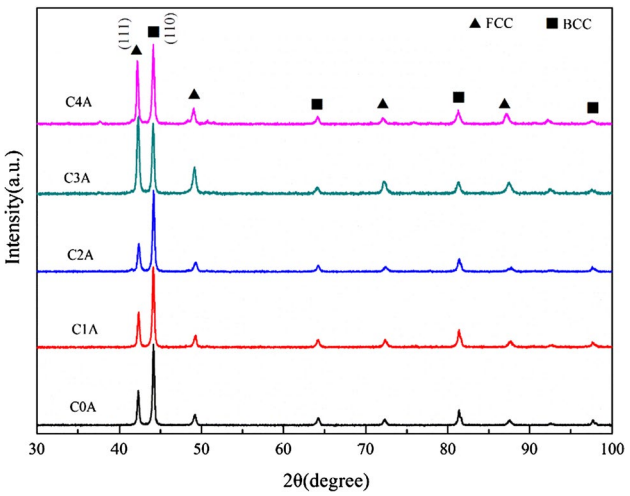

Fig. 6 XRD patterns of the annealed $Al_8(FeCuCrMn)_{92}C_x$ (marked as CxA) HEA strips

the chromium carbides were $Cr_{23}C_6$ particles, even smaller than 100 nm.

3.1.2 Microstructure of Annealed Strips

Figure 6 shows XRD patterns of $Al_8(FeCuCrMn)_{92}C_x$ strips after annealing at 1173 K for 2 h. In the annealed $Al_8(FeCuCrMn)_{92}C_x$ (denoted as CxA hereafter) strips, XRD patterns showed that, as in the as-cast samples, the bcc phase was major and fcc phase was minor. The intensity of the diffraction peak for fcc phase was greater with higher carbon content, indicating that carbon addition increased the fraction of fcc phase and modulated constituent phases in the annealed strips, as was in the as-cast strips. No diffraction peak of carbide phase was clearly observed from XRD patterns, not even in the C4A strip, suggesting that some carbides have dissolved during annealing such that the amount remained below the detectable limit of XRD.

Figure 7 exhibits microstrucutres of the annealed $Al_8(FeCuCrMn)_{92}C_x$ HEA strips. Annealing at 1173 K for 2 h had little influence on the main constituent phases of the strips prepared under near-rapid solidification. The C0A strip displayed a flower-like microstructure like that of the as-cast one. The C1A strip, however, clearly exhibited precipitation of carbide particles in bcc phase region. After annealing, the uneven distribution of fcc phase became more homogeneous in C3A and C4A strips, as the morphology of carbide particles changeed from fishbone to worm-like shapes. Statistical results suggested that the fraction of fcc phase in the annealed strips increased from 21 to 34 vol% after the addition of 4 at% carbon. Therefore, it is conclued that carbon addition modulated constituent phases in both as-cast and annealed $Al_8(FeCuCrMn)_{92}$ HEA strips by increasing the fraction of fcc phase.

Figure 8 shows elemental distribution maps of the C1A and the C3A strips. Chemical compositions of bcc and fcc phases in the annealed strips are listed in Table 2. Elemental distribution maps of the C1A and the C3A strips, like their cast counterparts, showed that the bcc phase was rich in Fe and Cr but poor in Cu, whereas the fcc phase was rich in Cu but poor in Fe and Cr. The difference in Al content between bcc phase and fcc phase, however, was smaller in the annealed strips than in the as-cast ones. For the other alloying elements, annealing increased the inhomogeneous between the two phases. The bcc phase contained just 1 at% Cu and the fcc phase contained almost 70 at% Cu, indicating that annealing had led to diffusion of Cu from the bcc phase to the fcc phase. The bcc phase contained more Mn in the annealed strips than in the as-cast ones. This uneven distribution was especially marked in the annealed strips with higher carbon content. The annealed samples also contained a higher number of carbides in the bcc phase, which apparently depleteed Cr in annealed strips. The higher the carbon content of a given strip, the lower the Cr measured in the bcc phase of that strip (Table 3).

3.1.3 Action Mechanism of Carbon on Microstructures

The experimental results strongly suggest that carbon addition can increase the fraction of fcc phase in both as-cast and annealed $Al_8(FeCuCrMn)_{92}C_x$ HEA strips. When the carbon content is 1 at%, $Cr_{23}C_6$-type carbides precipitate in the bcc phase. This is because Cr is a strong carbide-forming element and limits carbon solubility [34]. Both Cr and Mn are

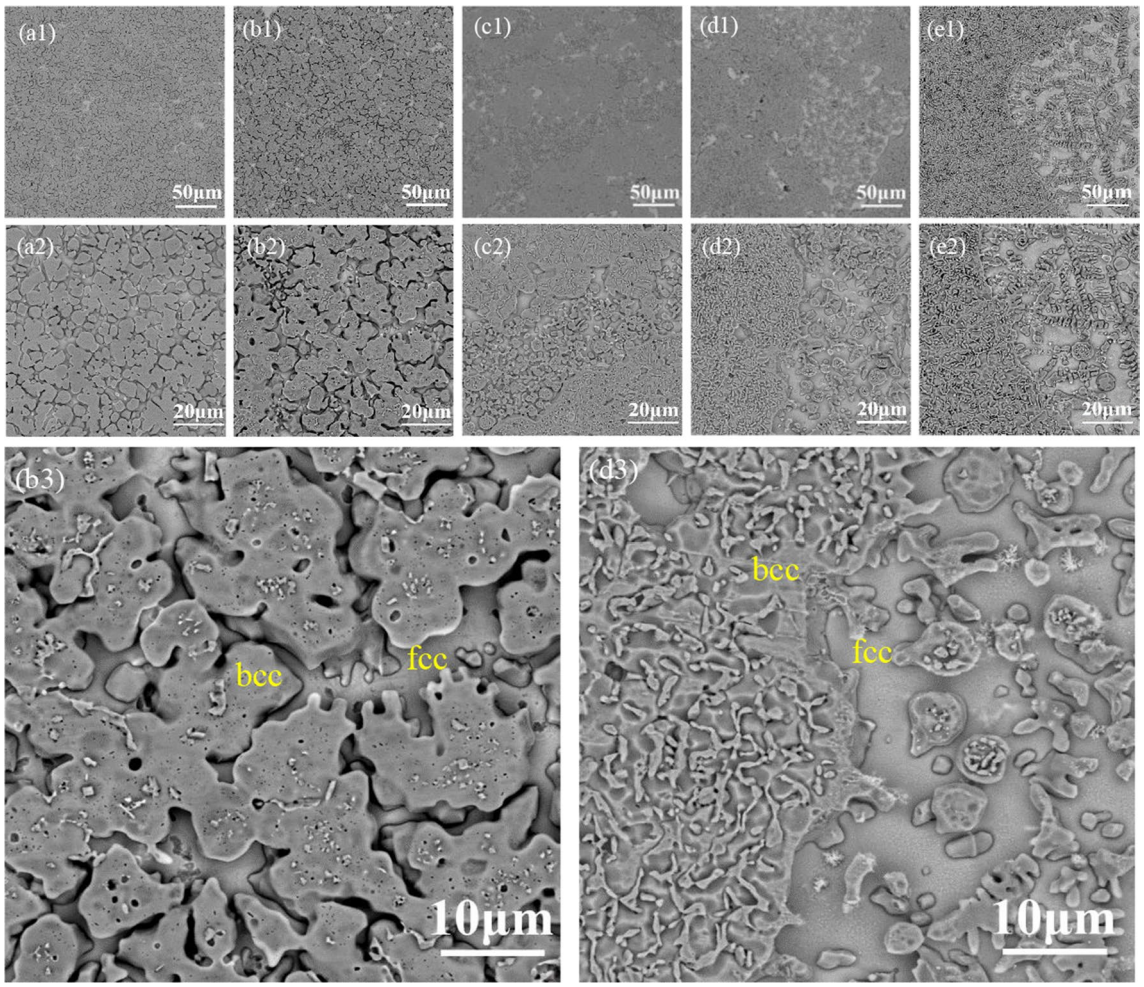

Fig. 7 Back-scattering SEM images of the annealed $Al_8(FeCuCrMn)_{92}C_x$ (marked as CxA) HEA strips: **a1**, **a2** for C0A strip, **b1**–**b3** for C1A strip, **c1**, **c2** for C2A strip, **d1**–**d3** for C3A strip, **e1**, **e2** for C4A strip

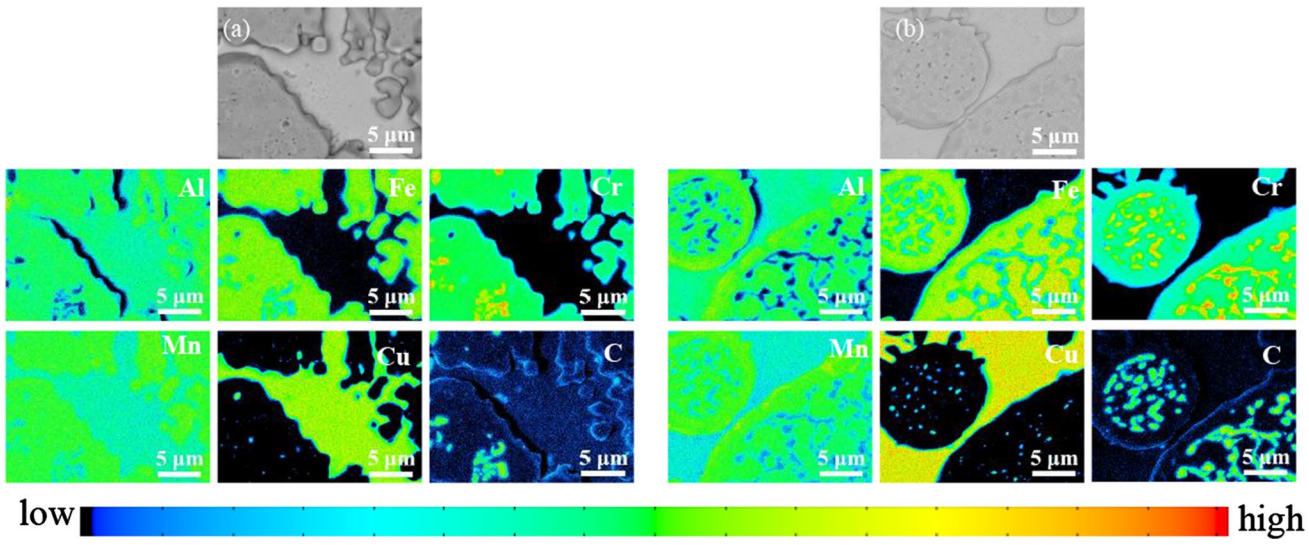

Fig. 8 Elemental distribution maps of the annealed $Al_8(FeCuCrMn)_{92}C_1$ and $Al_8(FeCuCrMn)_{92}C_3$ HEA strips: **a** C0A strip, **b** C3A strip

Table 2 Chemical compositions of bcc and fcc phases in the annealed $Al_8(FeCuCrMn)_{92}C_x$ HEAs derived from EPMA-EDS (since limited accuracy for light elements, carbon content is not listed here)

Sample	Phase	Al (at%)	Fe (at%)	Cu (at%)	Cr (at%)	Mn (at%)
C0A	bcc	6.8 ± 0.6	32.3 ± 2.4	1.4 ± 0.7	34.7 ± 1.3	23.8 ± 0.9
	fcc	7.1 ± 0.3	3.6 ± 0.4	69.0 ± 2.2	2.8 ± 0.3	17.5 ± 1.6
C1A	bcc	7.8 ± 0.8	33.5 ± 2.2	1.0 ± 0.8	32.9 ± 1.4	24.7 ± 0.8
	fcc	8.7 ± 1.2	3.2 ± 0.9	67.1 ± 1.8	2.1 ± 0.7	18.9 ± 0.9
C2A	bcc	7.4 ± 1.1	34.0 ± 1.5	1.1 ± 0.5	30.1 ± 1.6	26.2 ± 1.5
	fcc	7.3 ± 0.4	3.5 ± 1.8	68.9 ± 3.2	2.2 ± 0.6	18.1 ± 0.6
C3A	bcc	7.5 ± 1.2	33.9 ± 1.7	1.4 ± 0.6	25.2 ± 1.0	28.5 ± 1.9
	fcc	6.7 ± 0.3	2.9 ± 0.4	69.1 ± 1.1	1.4 ± 0.3	19.9 ± 1.2
C4A	bcc	8.1 ± 1.6	33.9 ± 0.3	1.3 ± 0.5	24.1 ± 1.7	31.8 ± 0.4
	fcc	7.8 ± 0.3	3.3 ± 1.7	68.5 ± 0.8	1.0 ± 0.1	19.4 ± 0.7

Table 3 Mixing enthalpy, ΔH_{mix}(KJ/mol), of atomic pairs among elements in the $Al_8(FeCuCrMn)_{92}C_x$ alloys

Element	Atomic radius (10^{-10} m)	Fe	Cu	Cr	Mn	C
Al	1.43	−11	−1	−10	−19	−36
Fe	1.24	–	13	−1	0	−50
Cu	1.28	–	–	12	4	−33
Cr	1.25	–	–	–	2	−61
Mn	1.29	–	–	–	–	−66
C	0.77	–	–	–	–	–

known to form carbides with C because the mixing enthalpy values of C–Cr and C–Mn are largely negative [31].

The atomic size difference δ of an alloy can be caculated by the following equation [2, 35]:

$$\delta = \sqrt{\sum_{i=1}^{n} c_i \left(1 - \frac{r_i}{\bar{r}}\right)^2} \quad (1)$$

$$\bar{r} = \sum_{i=1}^{n} c_i r_i \quad (2)$$

where n is the number of elements in an alloy, c_i is the atomic percentage of the i-th element, r is the average atomic radius, and r_i is the atomic radius of the i-th element. The atomic radius of carbon is much smaller than that of the other constituent elements. Based on Eqs. (1) and (2), the atomic size difference of HEAs increases as carbon content increases, thus decreasing solubility in solid solutions and resulting in the formation of a new phase, i.e. carbide [31, 36].

On the other hand, the mixing enthalpy values of Cu-Fe and Cu-Cr pairs are positive, which results in a Cu-rich fcc phase and a (Fe,Cr)-rich bcc phase. Figure 9 shows phase diagrams for $Al_8(FeCuCrMn)_{92}C_x$ HEA strips obtained by Thermo-Calc Software. Our calculated pseudo-binary diagram shows a miscibility gap and a monotectic reaction, i.e. Liquid → BCC + Liquid. We estimated ΔT, which is defined as $\Delta T = T_L - T_m$, where T_L is the liquid phase separation (LPS) temperature and T_m is the melting temperature [37, 38]. Wherever there exists a miscibility gap, LPS takes place. Our calculations indicate that when LPS occurs, the alloys separate into Cu-rich and Cu-poor liquid phases. This is similar to what occurs in other Cu-containing alloys, such as Cu-Nb [39], Cu-Fe [40] and Cu-Co-Fe [41, 42]. When our C1 strip was cooled, the miscibility gap ($\Delta T = 112$ K) caused the melt to separate into a Cu-rich fcc phase and a Cu-lean bcc phase, resulting in uneven distribution of Cu-rich fcc phase. As carbon content increased, the ΔT increased, i.e., the miscibility gap expanded and LPS occurred more readily. Our calculation of mole fraction changes of different phases in an $Al_8(FeCuCrMn)_{92}C_3$ HEA strip subjected to different temperatures showed that T_L and T_m were around 2104 K and 1590 K, respectively (Fig. 9c). The ΔT was therefore 514 K when carbon content was 3 at%. This large ΔT led to LPS and more uneven distribution of the Cu-rich fcc phase, even under conditions of near-rapid solidification, as displayed in Fig. 2b3 and d3. Therefore, carbon addition accelerated LPS, which in turn caused more uneven distribution of the Cu-rich fcc phase.

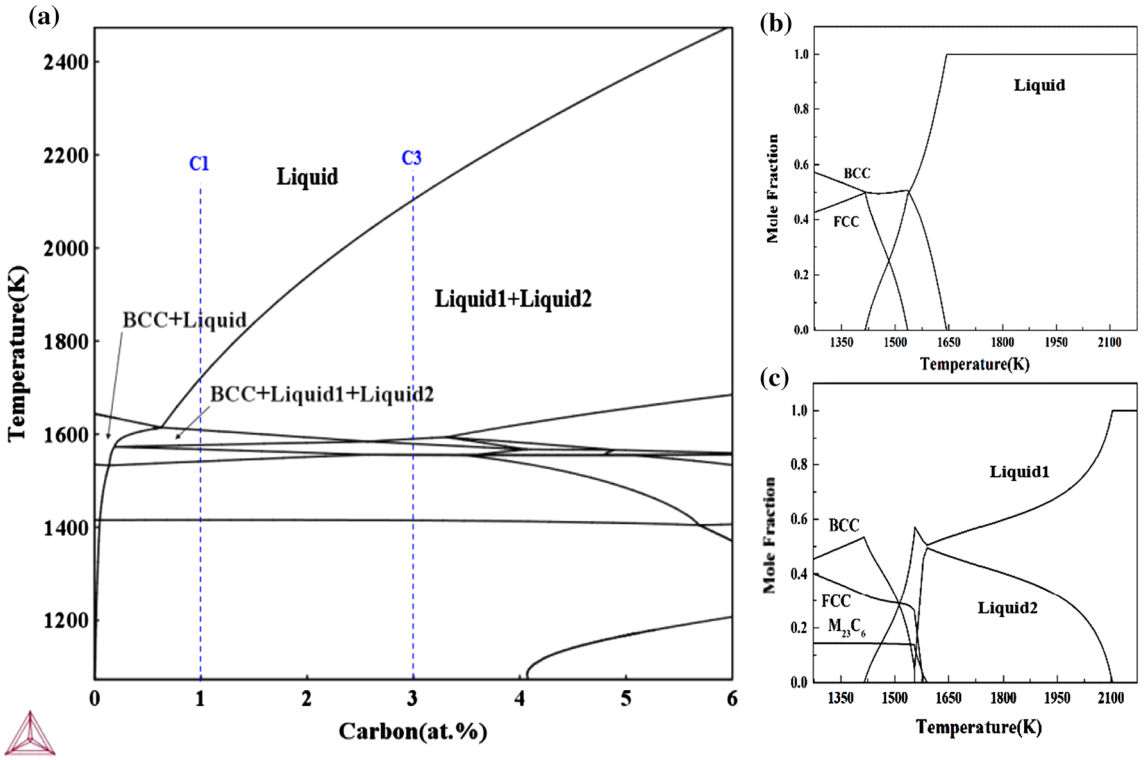

Fig. 9 Phase diagrams for $Al_8(FeCuCrMn)_{92}C_x$ HEA strips by Thermo-Calc Software: **a** Pseudo-binary phase diagram of $Al_8(FeCuCrMn)_{92}$-C system, **b** Mole fraction of different phases as temperatures in $Al_8(FeCuCrMn)_{92}C_1$ HEA strip, **c** Mole fraction of different phases as temperatures in $Al_8(FeCuCrMn)_{92}C_3$ HEA strip

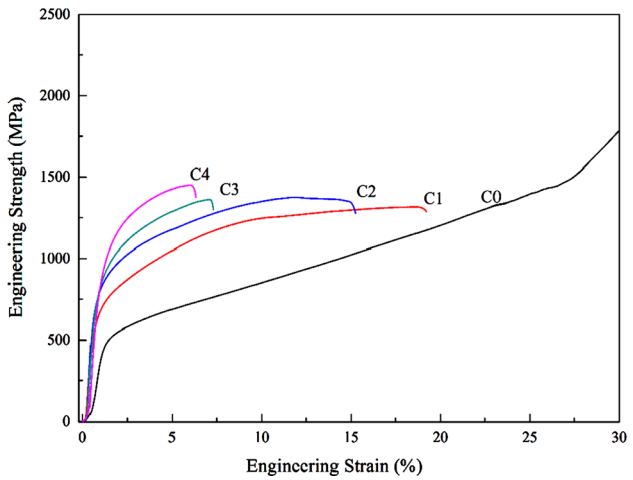

Fig. 10 Compressive mechanical properties of the as-cast $Al_8(FeCuCrMn)_{92}C_x$ HEA strips

3.2 Mechanical Properties

3.2.1 Mechanical Properties of As-Cast Strips

Figure 10 depicts engineering stress–strain compression curves for as-cast $Al_8(FeCuCrMn)_{92}C_x$ HEA strips. We extracted the values of yield strength, fracture strength, and fracture strain from these curves. These data showed that carbon addition enhanced yield strength from 512 MPa for the C0 strip to as high as 1023 MPa for the C4 strip (Table 4). The C0 strip showed no fracture, indicating very high ductility. With addition of carbon, fracture strain values were reduced to 19%, 15%, 7%, and 5% for the C1, C2, C3, and C4 strips, respectively. Thus, we concluded that carbon addition had improved yield at the cost of ductility, especially when carbon content reached 3 at%, at which point fracture strain value had decreased below 10%.

3.2.2 Mechanical Properties of Annealed Strips

Figure 11 shows compressive properties of the annealed $Al_8(FeCuCrMn)_{92}C_x$ strips. Yield strength, fracture strength and fracture strain of the annealed strips are listed in Table 4. The test results showed that carbon addition increased yield strength from 505 MPa for the C0A strip to 796 MPa for the C4A strip. Yield strength was reduced after annealing, but, C-added annealed strips maintained better ductility compared with the corresponding as-cast ones. In fact, the C1A strip, like both the C0 and C0A strips, remained completely free of compressive fracture. It is concluded that addition

Table 4 Compressive properties of as-cast and annealed $Al_8(FeCuCrMn)_{92}C_x$ HEA strips

Sample	As-cast					Annealed				
	C0	C1	C2	C3	C4	C0A	C1A	C2A	C3A	C4A
Yield strength (MPa)	512	672	796	859	1023	505	624	670	752	796
Fracture strength (MPa)	–	1312	1349	1361	1450	–	–	1624	1458	1423
Fracture strain (%)	No Fracture	19	15	7	5	No Fracture	No Fracture	20	16	9

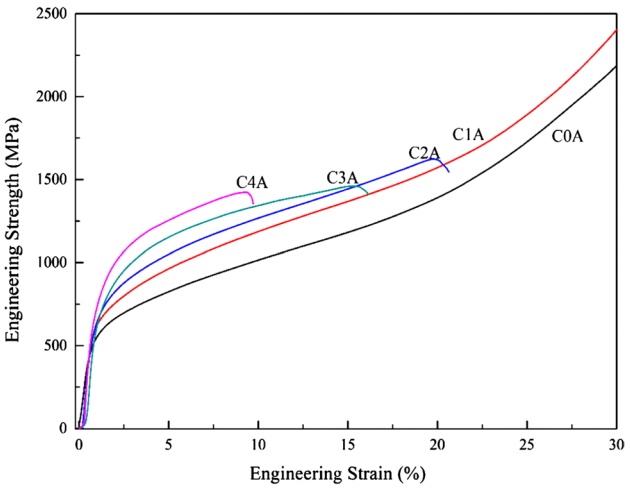

Fig. 11 Compressive mechanical properties of the annealed $Al_8(FeCuCrMn)_{92}C_x$ HEA strips

of 1 at% carbon with annealing at 1173 K for 2 h enhanced yield strength in $Al_8(FeCuCrMn)_{92}$ without loss of ductility.

3.2.3 Effect of Carbon on Mechanical Properties

After carbon addition to $Al_8(FeCuCrMn)_{92}C_x$ HEA strips, yield strength increases markedly. The yield strength (σ_y) of these strips can be decribed as follows [32]:

$$\sigma_y = \sigma_{fr} + \sigma_{in} + \sigma_{ss} + \sigma_{ppt} \quad (3)$$

where σ_{fr} is lattice friction stress, σ_{in}, σ_{ss} and σ_{ppt} are the strengthening contributions from interfaces, solid solutions and precipitates, respectively. In our alloys, σ_{in} results from the interfaces between bcc and fcc phases and grain boundaries [43–45]. Microstructure examination showed that interface density became higher in strips with higher carbon content, indicating that interface strengthening contribute to strength enhancement. In HEAs, it is difficult to distinguish the solvent from the solute because the consituent atoms of the alloy are distributed randomly throughout the lattice. Therefore, the value for σ_{ss} is commonly embedded into σ_{fr} [32, 46]. Lattice distortions are introduced by carbon addition, whose atomic radius is small [24, 47–50]. Since the number of carbides is low in the C1 strip, the majority of the increase in yield strength is ascribed to the increase in σ_{ss} [21]. On the other hand, as carbon content increased, additional carbides were precipitated in the bcc phase region, and the resulting precipitation strengthening further improved yield strength. We thus concluded that the enhanced yield strength observed in the as-cast $Al_8(FeCuCrMn)_{92}$ HEA strip after carbon addition was the result of both interstitial solid solution strengthening and precipitation strengthening.

The fraction of fcc phase is relatively high in strips with high carbon content, which would normally be beneficial for ductility [24]. We found, however, that carbon addition causes reduction in ductility of the as-cast $Al_8(FeCuCrMn)_{92}$ HEA strips because of uneven distribution of fcc phase. When carbon content was increased beyond 2 at%, the increasingly uneven distribution of fcc phase, along with the increasing size and number of carbides long certain boundaries, resulted in sharply decreasing ductility due to the extreme unevenness of stress distribution [47, 51–54].

After annealing at 1173 K for 2 h, the yield strength of all HEA strips decreased to some extent, but the yield strength of the C-added strips was still higher than that of the C-free strip. The ductilty of all the C-added strips was improved by annealing. The fraction of fcc phase did not clearly change after annealing, but thermal stress is relieved [55]. XRD patterns also showed that diffraction peaks for certain carbides had disappeared, indicating that some carbides had dissolved, and SEM images showed that the morphology of the remaining carbides had changed from fishbone-like to worm-like shapes. Since all these factors contribute to improvement of ductility, we conclude that annealing had improved the ductility of our $Al_8(FeCuCrMn)_{92}C_x$ HEA strips. The C1A strip also showed no fracture during compression, we therefore concluded that optimized carbon content addition with annealing brought about marked improvement of the yield strength of our bcc matrix $Al_8(FeCuCrMn)_{92}$ HEA strips without any loss of ductility.

4 Conclusions

We studied the effect of interstitial carbon on the microstructure and the mechanical properties of bcc matrix $Al_8(FeCuCrMn)_{92}$ HEA strips. We concluded the following:

1. The as-cast $Al_8(FeCuCrMn)_{92}$ HEA strip prepared under near-rapid solidification had 17 vol% of Cu-rich fcc phase embedded in a (Fe, Cr)-rich bcc phase matrix. Carbon addition modulated constituent phases by increasing the fraction of fcc phase, but also led to the uneven distribution of this phase in the bcc matrix.
2. Carbon addition enhanced yield strength of the as-cast HEA strips by introducing both interstitial solution strengthening and precipitation strengthening. At the same time, however, carbon addition decreased the ductility because of the precipitation of needle-like or fishbone-like carbides in the bcc phase region and the uneven distribution of the fcc phase.
3. After annealing at 1173 K for 2 h, the main constituent phases of our $Al_8(FeCuCrMn)_{92}$ HEA strips were similar to the as-cast ones, but their ductility was markedly improved. We attributed this result to several factors: (a) the volume fraction of fcc phase remained high in these alloys, (b) thermal stress was relieved by annealing, and (c) certain carbides dissolved, while the morphology of those remaining was shifted from fishbone-like to worm-like shapes.
4. Addition of carbon to an optimized level of 1 at% achieved an improvement of 30% in the yield strength of our annealed bcc matrix $Al_8(FeCuCrMn)_{92}$ HEA strip without any loss of ductility.

Acknowledgements This work was financially supported by the National Natural Science Foundation of China (No. 51974184) and National MCF Energy R&D Program of China (No. 2018YFE0306102). The authors would like to express sincere thanks to the scientific and technical support from the Instrumental Analysis & Research Center at Shanghai University. A portion of work was performed at the National High Magnetic Field Laboratory, USA, which is supported by National Science Foundation Cooperative Agreement [Grant No. NSF DMR-1644779] and the State of Florida, USA. The authors are grateful to Mary Tyler for editing.

References

1. J.W. Yeh, S.K. Chen, S.J. Lin, J.Y. Gan, T.S. Chin, T.T. Shun, C.H. Tsau, S.Y. Chang, Adv. Eng. Mater. **6**, 299 (2004)
2. Y. Zhang, T.T. Zuo, T. Zhi, M.C. Gao, K.A. Dahmen, P.K. Liaw, Z.P. Lu, Prog. Mater. Sci. **61**, 1 (2014)
3. E.J. Pickering, N.G. Jones, Int. Mater. Rev. **61**, 183 (2016)
4. D.B. Miracle, O.N. Senkov, Acta Mater. **122**, 448 (2017)
5. M.A. Hemphill, T. Yuan, G.Y. Wang, J.W. Yeh, C.W. Tsai, A. Chuang, P.K. Liaw, Acta Mater. **60**, 5723 (2012)
6. Z. Tang, T. Yuan, C.W. Tsai, J.W. Yeh, C.D. Lundin, P.K. Liaw, Acta Mater. **99**, 247 (2015)
7. M.H. Chuang, M.H. Tsai, W.R. Wang, S.J. Lin, J.W. Yeh, Acta Mater. **59**, 6308 (2011)
8. N.A.P. Kiran Kumar, C. Li, K.J. Leonard, H. Bei, S.J. Zinkle, Acta Mater. **113**, 230 (2016)
9. Y.D. Wu, Y.H. Cai, T. Wang, J.J. Si, J. Zhu, Y.D. Wang, X.D. Hui, Mater. Lett. **130**, 277 (2014)
10. M.J. Chae, A. Sharma, M.C. Oh, B. Ahn, Met. Mater. Int. **27**, 629 (2021)
11. C. Ng, S. Guo, J. Luan, S. Shi, C.T. Liu, Intermetallics **31**, 165 (2012)
12. O.N. Senkov, G.B. Wilks, D.B. Miracle, C.P. Chuang, P.K. Liaw, Intermetallics **18**, 1758 (2010)
13. S. Guo, C. Ng, J. Lu, C.T. Liu, J. Appl. Phys. **109**, 103505 (2011)
14. Y. Lu, Y. Dong, S. Guo, L. Jiang, H. Kang, T. Wang, B. Wen, Z. Wang, J. Jie, Z. Cao, H. Ruan, T. Li, Sci. Rep. **4**, 6200 (2014)
15. Y.J. Zhou, Y. Zhang, Y.L. Wang, G.L. Chen, Appl. Phys. Lett. **90**, 181904 (2007)
16. S. Sheikh, S. Shafeie, Q. Hu, J. Ahlström, C. Persson, J. Veselý, J. Zýka, U. Klement, S. Guo J. Appl. Phys. **120**, 164902 (2016)
17. H. Huang, Y. Wu, J. He, H. Wang, X. Liu, K. An, W. Wu, Z. Lu, Adv. Mater. **29**, 1701678 (2017)
18. Y. Zou, S. Maiti, W. Steurer, R. Spolenak, Acta Mater. **65**, 85 (2014)
19. Y. Wang, Y. Yang, H. Yang, Z. Min, J. Qiao, J. Alloy. Compd. **725**, 365 (2017)
20. Z. Li, Acta Mater. **164**, 400 (2019)
21. Z. Wang, I. Baker, Mater. Lett. **180**, 153 (2016)
22. O.A. Lukianova, Z. Rao, V. Kulitckii, Z. Li, G. Wilde, S.V. Divinski, Scripta Mater. **188**, 264 (2020)
23. F. Yang, R. Song, Y. Li, T. Sun, K. Wang, Mater. Design **76**, 32 (2015)
24. Z. Wang, I. Baker, Z. Cai, S. Chen, J.D. Poplawsky, G. Wei, Acta Mater. **120**, 228 (2016)
25. C.H. Hu, J.L. Zhang, Y.H. Zhang, H. Ke, C.M. Li, C.J. Song, Q.J. Zhai, J. Iron Steel Res. Int. **25**, 877 (2018)
26. J.T. Fan, L.J. Zhang, P.F. Yu, M.D. Zhang, D.J. Liu, Z. Zhou, P. Cui, M.Z. Ma, Q. Jing, G. Li, R.P. Liu, Mater. Sci. Eng. A **728**, 30 (2018)
27. Q. Zhang, H. Xu, X.H. Tan, X.L. Hou, S.W. Wu, G.S. Tan, L.Y. Yu, J. Alloy. Compd. **693**, 1061 (2017)
28. A. Verma, P. Tarate, A.C. Abhyankar, M.R. Mohape, D.S. Gowtam, V.P. Deshmukh, T. Shanmugasundaram, Scripta Mater. **161**, 28 (2019)
29. R. Kulkarni, B.S. Murty, V. Srinivas, J. Alloy. Compd. **746**, 194 (2018)
30. J.L. Zhang, C.H. Hu, Y.H. Zhang, J.H. Li, C.J. Song, Q.J. Zhai, Mater. Design **186**, 108307 (2020)
31. N.D. Stepanov, N.Y. Yurchenko, M.A. Tikhonovsky, G.A. Salishchev, J. Alloy. Compd. **687**, 59 (2016)
32. Z. Wang, I. Baker, W. Guo, J.D. Poplawsky, Acta Mater. **126**, 346 (2017)
33. S. Downey II, P.N. Kalu, K. Han, Mater. Sci. Eng. A **480**, 96 (2008)
34. A. Takeuchi, A. Inoue, Mater. Trans. **46**, 2817 (2005)
35. C.H. Chen, Y.J. Chen, J.J. Shen, Met. Mater. Int. **26**, 617 (2020)
36. M.B. Kivy, C.S. Kriewall, M.A. Zaeem, Mater. Res. Lett. **6**, 321 (2018)
37. W. Zhai, L. Hu, K. Zhou, B. Wei, J. Phys. D Appl. Phys. **49**, 165306 (2016)
38. A. Munitz, M.J. Kaufman, R. Abbaschian, Intermetallics **86**, 59 (2017)
39. A. Munitz, M. Bamberger, A. Venkert, P. Landau, R. Abbaschian, J. Mater. Sci. **44**, 64 (2009)
40. Y.Z. Chen, F. Liu, G.C. Yang, X.Q. Xu, Y.H. Zhou, J. Alloy. Compd. **427**, L1 (2007)
41. A. Munitz, R. Abbaschian, J. Mater. Sci. **33**, 3639 (1998)
42. A. Munitz, A.M. Bamberger, S. Wannaparhun, R. Abbaschian, J. Mater. Sci. **41**, 2749 (2006)
43. Z. Wang, I. Baker, Mater. Sci. Eng. A **693**, 101 (2017)

44. K. Han, R. Goddard, R. Niu, T. Li, D.N. Nguyen, J.R. Michel, J. Lu, V. Pantsyrny, IEEE Trans. Appl. Supercon. **26**, 8400804 (2016)
45. K. Han, V.J. Toplosky, R. Walsh, C.A. Swenson, IEEE Trans. Appl. Supercon. **12**, 1176 (2002)
46. A. Böttger, M.L. Genderen, K. Han, E.J. Mittemeijer, J. Phys. IV France **7**, 257 (1997)
47. L. Cheng, A. Böttger, T.H. Keijser, E.J. Mittemeijer, Scripta Mater. **24**, 509 (1990)
48. K. Han, M.J. Genderen, A. Böttger, H.W. Zandbergen, E.J. Mittemeijer, Philos. Mag. A **81**, 741 (2001)
49. K.A. Taylor, L. Chang, G.B. Olson, G.D.W. Smith, M. Cohen, J.B.V. Sande, Metall. Mater. Trans. A **20**, 2717 (1989)
50. K.A. Taylor, M. Cohen, Prog. Mater. Sci. **36**, 151 (1992)
51. K. Han, V. Toplosky, N. Min, J. Lu, Y. Xin, R. Walsh, IEEE Trans. Appl. Supercon. **28**, 0602405 (2018)
52. K. Han, D.V. Edmonds, G.D.W. Smith, Metall. Mater. Trans. A **32**, 1313 (2001)
53. K. Han, T.D. Mottishaw, G.D.W. Smith, D.V. Edmonds, Mater. Sci. Technol. **10**, 955 (1994)
54. K. Han, G.D.W. Smith, D.V. Edmonds, Metall. Mater. Trans. A **26**, 1617 (1995)
55. K. Masemola, P. Popoola, N. Malatji, J. Mater. Res. Technol. **9**, 5241 (2020)

Publisher's Note Springer Nature remains neutral with regard to jurisdictional claims in published maps and institutional affiliations.